Journal of Molecular Graphics and Modelling 38 (2012) 446–454

Contents lists available at SciVerse ScienceDirect

Journal of Molecular Graphics and Modelling

journal homepage: www.elsevier.com/locate/JMGM

The C-terminal domain of the 2b protein of *Cucumber mosaic virus* is stabilized by divalent metal ion coordination

Ákos Gellért[a,*], Katalin Nemes[b,c], Katalin Kádár[a,d], Katalin Salánki[c], Ervin Balázs[a]

[a] *Agricultural Institute, Centre for Agricultural Research, Hungarian Academy of Sciences, Department of Applied Genomics, Brunszvik Rd. 2, H-2462 Martonvásár, Hungary*
[b] *Department of Plant Pathology, Corvinus University of Budapest, Ménesi Rd. 44, H-1118 Budapest, Hungary*
[c] *Agricultural Biotechnology Center, Szent-Györgyi Albert Str. 4, H-2100 Gödöllő, Hungary*
[d] *Szent István University, Páter Károly Str. 1, H-2103 Gödöllő, Hungary*

ARTICLE INFO

Article history:
Received 4 April 2012
Received in revised form 10 August 2012
Accepted 13 August 2012
Available online 10 October 2012

Keywords:
Cucumoviruses
CMV 2b protein
Protein structure prediction
Molecular dynamics simulation
Metal ion binding site
Intrinsically disordered proteins

ABSTRACT

The main function of the 2b protein of *Cucumber mosaic virus* (CMV) is binding permanently the double stranded siRNA molecules in the suppression process of post-transcriptional gene silencing (PTGS). The crystal structure of the homologue *Tomato aspermy virus* (TAV) 2b protein is known, but without the C-terminal domain. The biologically active form is a tetramer: four 2b protein molecules and two siRNA duplexes. Regarding the complete 2b protein structure, we performed a molecular dynamics (MD) simulation of the whole siRNA–2b ribonucleoprotein complex. Unfortunately, the C-terminal domain is proved to be partially unstructured. Multiple sequence alignment showed a well conserved motif between residues 94 and 105. The negatively charged residues of the C-terminal domain are supposed to take part in coordination of a divalent metal ion and stabilize the three-dimensional structure of the C-terminal domain. MD simulations were performed on the detached C-terminal domains (aa 65–110). 0.15 M $MgCl_2$, $CaCl_2$, $FeCl_2$ and $ZnCl_2$ salt concentrations were used in the screening simulations. Among the tested divalent metal ions Mg^{2+} proved to be very successful because Asp95, Asp96 and Asp98 forms a quasi-permanent Mg^{2+} binding site. However the control computations have resulted in any (at least) divalent metal ion remains in the binding site after replacement of the bound Mg^{2+} ion. A quadruple mutation (Rs2DDTD/95–98/AAAA) was introduced into the position of the putative divalent metal ion binding site to analyze the biological relevance of molecular modeling derived hypothesis. The plant inoculation experiments proved that the movement of the mutant virus is slower and the symptoms are milder comparing to the wild type virus. These results demonstrate that the quadruple mutation weakens the stability of the 2b protein tetramer–siRNA ribonucleoprotein complex.

1. Introduction

Cucumber mosaic virus (CMV) and *Tomato aspermy virus* (TAV) belong to the *Cucumovirus* genus in the family *Bromoviridae* [1]. CMV infects over a thousand plant species and cause serious crop losses in agriculture, principally in vegetable and ornamental cultures while the host-plant range of TAV is significantly narrower. The genome of cucumoviruses consists of three single-stranded, positive-sense RNA molecules and codes for five viral proteins. Elements of the viral replication complex, protein 1a and 2a, are encoded by RNA 1 and 2. RNA 2 encodes for another small protein (2b) in a shifted and overlapped open reading frame (ORF), which has a key role in the suppression of RNA silencing and takes part in the regulation/induction of symptom expression [2]. RNA 3 encodes the movement protein (3a, MP) and coat protein (3b, CP). The main function of the CP is to encapsidate the viral RNA while the MP participates in the transport of the pathogen to the adjacent plant cell through plasmodesmata [3–5]. The virus particle of *cucumoviruses* is assembled from 180 CP subunits with a $T = 3$ truncated icosahedral symmetry [2,6,7].

The structure of the smallest cucumovirus coded protein, 2b, is mainly alpha helical and it is composed of 110 amino acids (aa). During viral infection it is localized in the nucleus [8]. The major function of the 2b protein of *cucumoviruses* is to bind permanently the double stranded siRNA molecules to suppress the post-transcriptional gene silencing (PTGS) process [9–11]. The crystal structure of the homologue TAV 2b protein is already known [12], but the structure of the C-terminal domain (aa 69–110) is absent. The C-terminal domain is proved to be toxic when it was expressed in *Escherichia coli* [13]. The known part of the 2b protein

* Corresponding author. Tel.: +36 22 569 500x317; fax: +36 22 569 514.
E-mail addresses: gellert.akos@agrar.mta.hu (Á. Gellért), nemeskat@yahoo.com (K. Nemes), kadark@mail.mgki.hu (K. Kádár), salanki@abc.hu (K. Salánki), balazs.ervin@agrar.mta.hu (E. Balázs).

1093-3263/$ – see front matter © 2012 Elsevier Inc. All rights reserved.
http://dx.doi.org/10.1016/j.jmgm.2012.08.005

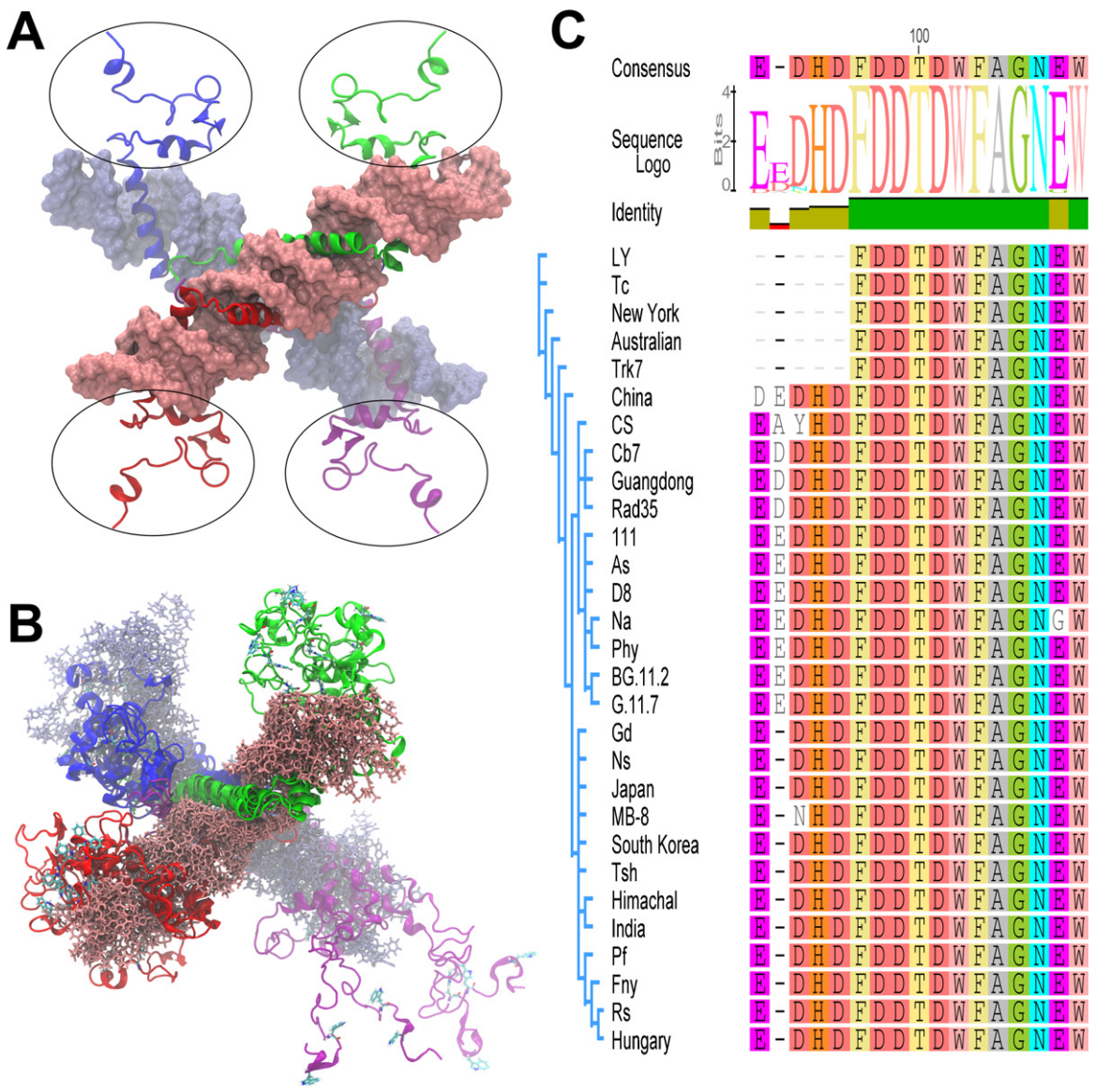

Fig. 1. Structure of the siRNA–2b tetramer ribonucleoprotein complex and the conserved sequence motif between position 94 and 105. The modeled C-terminal domains are encircled. The protein chains of the complex are in cartoon while siRNA duplexes are in molecular surface representation (A). Snapshots of the simulated siRNA–2b tetramer, every 8 ns were superimposed. It can be seen that the C-terminal domain and the siRNA ends become partially unfolded, furthermore the Trp99 and Trp105 residues do not to coordinate to siRNA endings (B). Multiple sequence alignment of 29 different CMV 2b protein sequences (C).

contains two long α-helices. The helical axes are rotated by 120° around each other. The 2b protein forms a pair of hook-like dimers to bind the siRNA duplex. The α-helices fit into the major groove of the siRNA in a sequence-independent and length-preference manner. The biologically active form is a tetramer (Fig. 1A), which is formed by four 2b protein molecules and two siRNA duplexes.

Mainly electrostatic interactions take place between the positively charged protein side chains and the RNA sugar-phosphate backbone at the RNA–protein interface. There is a π–π stacking effect between the conserved Trp50 and the 5′-terminal base, as observed in the TAV 2b X-ray structure [12].

Multiple sequence alignment showed that leucine is conserved at position 50 in numerous CMV strains. Another plant virus protein the *Carnation Italian ringspot virus* (CIRV) p19 binds 21 nt siRNA in a size selective manner where Trp39 and Trp42 act as end-capping residues with the base pairs on each end of the siRNA fragment [14]. The first defective interfering RNA molecule in *Cymbidium ringspot virus* infections was reported by Burgyán et al. [15].

There are also two conserved tryptophans in CMV 2b sequences at position 99 and 105 and these residues may have similar RNA stabilizing function as in CIRV p19 (Fig. 1C). Therefore, in order to gain further insight into the functional and structural features of the siRNA bound 2b tetramer, we performed molecular dynamics (MD) simulations to check the role of the conserved Trp99 and Trp105. Unfortunately the CMV 2b C-terminal domain have become partially unstructured during simulations and we could not detect π–π stacking formation between tryptophan residues and terminal siRNA bases (Fig. 1B). Then, we identified a well-conserved DDTD motif in the sequence alignment at position 95–98 which probably form a divalent metal ion binding site in the 2b C-terminal domain. In order to identify which type of metal ions can bind permanently to this putative site we tested four divalent metal ions. Individually 32–32 ns long MD simulations were performed on the separate C-terminal domain model (aa 65–110) and the system was filled up with 0.15 M $MgCl_2$, $CaCl_2$, $FeCl_2$, $ZnCl_2$, respectively. These MD simulations showed that the 2b C-terminal domain is stabilized by a bound Mg^{2+} ion while the other studied metal ions did not show

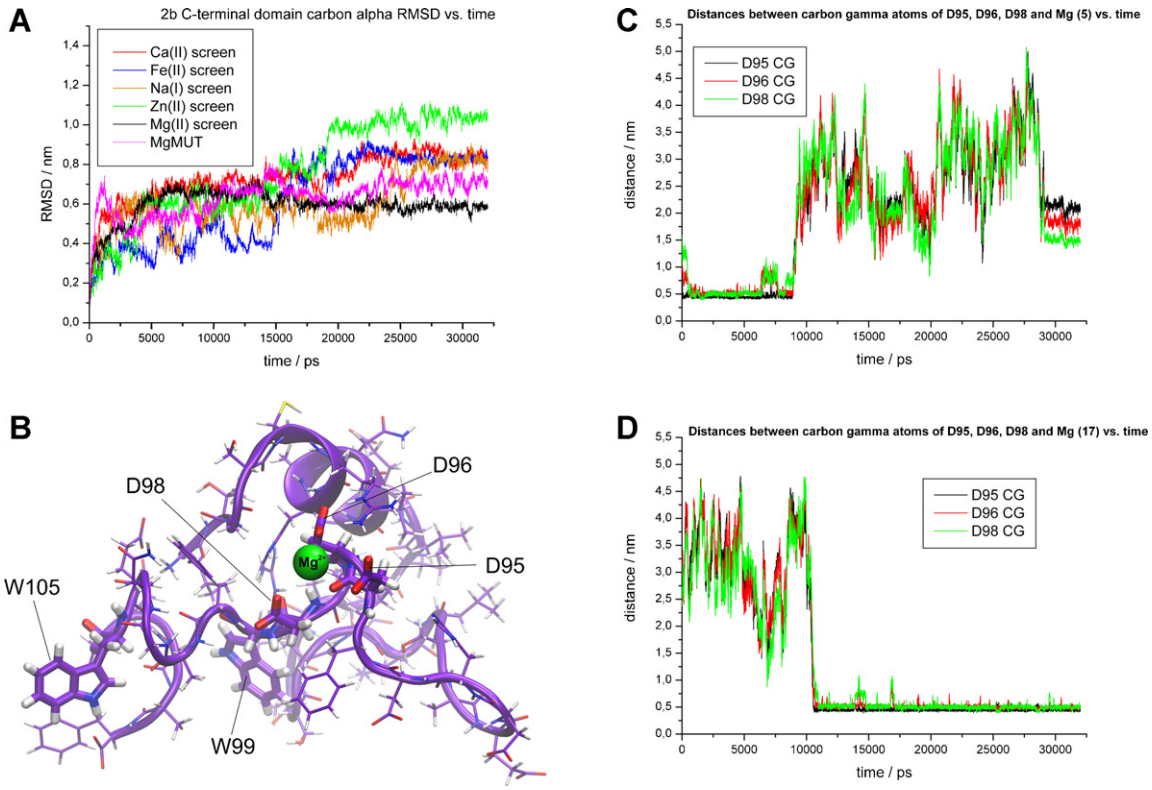

Fig. 2. Analysis of the CMV 2b C-terminal domain MD simulations. The initial structures were taken as references when calculating RMSD values. Solely the Mg^{2+} (black line) screen took the system into dynamic equilibrium state which is clearly visible from the RMSD plot. Abbreviation of the Rs2DDTD/95–98/AAAA mutant 2b C-terminal Mg^{2+} screen is MgMUT (A). A snapshot structure of the 2b C-terminal domain from the equilibrium state. The protein part is in cartoon and licorice representation. Aspartate residues which take part in the Mg^{2+} coordination are thicker (B). Retention times of two Mg^{2+} ions. Mg^{2+} number 5 was coordinated by D95, D96 and D98 residues during the first third of the simulation then Mg^{2+} number 17 was coordinated until the end of the simulation (C and D).

such effect (Fig. 2A and B). In order to make sure that the binding of Mg^{2+} ion was not only by chance, 100 ns long control MD simulations were run where the bound Mg^{2+} was exchanged for Ca^{2+}, Fe^{2+} and K^{+} ions. Finally, a quadruple mutation (Rs2DDTD/95–98/AAAA) was introduced into the infectious clone of Rs-CMV at the position of the putative divalent metal ion binding site to check the biological relevance of the above mentioned molecular modeling derived hypothesis.

2. Methods and materials

2.1. Prediction of the full length 2b protein structure

The three-dimensional structure of the full-length monomer CMV 2b was generated with I-TASSER [16,17]. The model was built using the Rs-CMV 2b sequence. The NCBI/GenBank accession number is AJ517801. The main template was the X-ray structure of TAV 2b (PDB ID code: 2ZI0) to create the alpha helical regions (aa 1–69). Structure of the F(1)-ATPase from spinach chloroplasts (PDB ID: 1FX0) and structure of the Glia cell missing (GCM) transcription factor (PDB ID: 1ODH) were used to thread the model structure of the CMV 2b C-terminal domain (aa 65–110). The result page of the I-TASSER structure prediction includes the detailed sequence alignments (see Supplementary Fig. S1 online). The biologically active tetramer form and siRNA duplexes (sequence of the 32 nt siRNA is described in the supplement of [12]) was built with the Schrödinger Suite [18] molecular modeling software package. The completed tetramer–siRNA ribonucleoprotein complex was refined with energy minimization to eliminate the steric conflicts between the protein and RNA atoms.

2.2. Molecular dynamics and graphics

Prior to MD simulations the Desmond system building panel (incorporated into Schrödinger Suite) was used to construct the solvated siRNA–2b tetramer ribonucleoprotein complex and the solvated 2b C-terminal domains for metal ion binding simulations. Accordingly 0.15 M $MgCl_2$, $CaCl_2$, $FeCl_2$, $ZnCl_2$ and NaCl salt concentrations were used for the metal ion binding screens. The detailed compositions for all simulated systems are summarized in Table 1. The OPLS-AA/2005 force field was used in all simulations. Before starting the production runs the systems were prepared with energy minimizations and short restrained MD simulations: first, only the position of the solvent molecules was minimized and then the potential energy of the whole system without any restraints. In the subsequent step on an NVT ensemble, a short 12 ps position-restrained MD simulation at 10 K was carried out using a Berendsen thermostat to ensure the proper solute settlement around the protein. After this, 12 ps of position restrained MD simulation were performed on an NPT ensemble at 10 K and 1 bar using a Berendsen thermostat and pressure coupling. Then a 12 ps restrained NPT MD simulation warmed the solute to 300 K at 1 bar. Finally, a 24 ps non restrained NPT MD simulation prepared the systems for the production run at 300 K and 1 bar.

The MD simulations were initiated on the NPT ensemble 300 K and 1 bar using the Desmond [19] molecular dynamics software application. The simulations were evaluated by the Desmond "simulation event analysis" application package of the Schrödinger Suite. The computing capacities were around 8.5 and 0.8 ns/day for the C-terminal domain and the tetramer–siRNA ribonucleoprotein complex simulation, respectively. MD simulations were performed on IntelXeon server clusters using sixteen parallel processor cores.

Table 1
Composition summary of the simulated systems.

	System name								
	Full system[a]	C-terminal Ca(II) screen	C-terminal Fe(II) screen	C-terminal Na(I) screen	C-terminal Zn(II) screen	C-terminal Mg(II) screen	Mutant C-terminal Mg(II) screen	Bonded Ca^{2+} control	Bonded Fe^{2+} control	Bonded K^+ control
Simulation box volume (nm^3)	2625.942	232.327	232.327	232.327	232.327	232.327	232.327	232.327	232.327	232.327
Number of protein atoms	7048	676	676	676	676	676	666	676	676	676
Number of RNA atoms	4088	–	–	–	–	–	–	–	–	–
Number of water (TIP3P) molecules	78,497	7134	7118	7166	7143	7155	7175	7162	7120	7153
Number of neutralizing Na^+ ions	104	8	8	8	8	8	5	6	6	7
Number of metal ions	219 Na^+	20 Ca^{2+}	20 Fe^{2+}	20 Na^+	20 Zn^{2+}	20 Mg^{2+}	20 Mg^{2+}	1 Ca^{2+} 20 Mg^{2+}	1 Fe^{2+} 20 Mg^{2+}	1 K^+ 20 Mg^{2+}
Number of Cl^- ions	219	40	40	20	40	40	40	40	40	40
Salt concentration (mol/L)	0.155	0.156	0.156	0.155	0.155	0.155	0.155	0.155	0.155	0.155
Simulation time (ns)	32	32	32	32	32	32	32	100	100	100

[a] Tetramer 2b protein complexed with two 32 nt long siRNA duplex.

Fig. 3. Ribbon image of the 2b C-terminal domain. The five substructural elements are colored separately: the α-helix is magenta, the short β-sheet is yellow, the loop region is menthol green, the divalent metal ion binding site is pale blue while the C-terminal tail is violet. It is worth noticing that the metal ion binding site is located in the center of the C-terminal domain structure.

Electrostatic potential map was calculated with Adaptive Poisson–Boltzmann Solver version 1.3 [20] (APBS) using the linearized Poisson–Boltzmann method [21] with a dielectric constant of 78.54 and 2 for the water solvent and protein core, respectively. The coordinated Mg^{2+} ion was removed before calculation. We used the VMD software [22] to create spectacular molecular graphics.

2.3. Plasmid constructs

Description of the Rs-CMV and the infectious transcripts (pRs1, pRs2, pRs3) has been published previously [23]. The recombinant RNA 2 clone, pRs2DDTD/95–98/AAAA was generated by PCR-based mutagenesis of pRs2 using the following oligonucleotide primers: forward 5′-GG**GCTGCAGCGGCT**TGGTTCGCCGGT-3′ and reverse 5′-GGCGCTGCAGCAAAATCATGGTCTTC-3′. The restriction endonuclease site (PstI) is underlined and the mutated nucleotides are written in bold.

Fig. 4. Electrostatic field around the CMV 2b C-terminal domain. Electric field lines indicate the presence of a channel toward to the Mg^{2+} binding site. Electric filed visualization parameters in VMD: gradient magnitude is 2.7, minimal length is 7.24 and maximal length is 32.19.

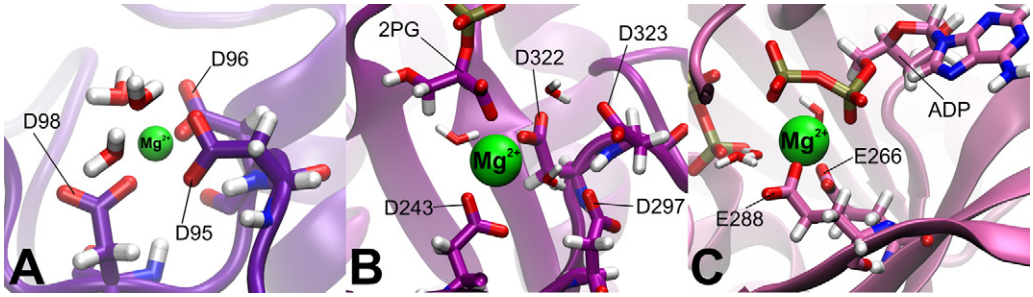

Fig. 5. Comparison of magnesium binding sites. The newly discovered putative divalent metal ion binding site on the CMV 2b C-terminal domain (A). Active site of the Entamoeba histolytica enolase (PDB ID code: 3QTP). Here the Mg^{2+} is surrounded with aspartate side chains, water molecules and the substrate (B). Active site of *Escherichia coli* carboxylase (PDB ID code: 3RV3). The main difference is that the Mg^{2+} ion is coordinated by glutamate residues (C).

2.4. Plant growth and inoculation

Nicotiana clevelandii Gray and *Nicotiana glutinosa* L. plants were kept in environmentally controlled growth chambers at cycle of 14 h of light (23 °C) and 10 h of dark (18 °C). The plants were mechanically inoculated at the fourth-leaf stage with *in vitro* mutated RNA2 transcripts in the presence of wild type RNA 1 and 3 transcripts or RNA 1, 2 and 3 of the wild type Rs-CMV transcripts. Symptom development was observed and recorded continuously during the following 2 weeks.

2.5. Analysis of plants

Total RNA was extracted from 200 mg systemically infected leaves 4 and 8 days after inoculation [24]. Virus RNA accumulation was followed by Northern blot analysis. Approximately 100 ng total RNA was denatured with formaldehyde and separated in formamide-containing agarose gels and blotted on to nylon membranes [25]. Northern blot hybridization analysis was performed with random-primed ^{32}P-labeled DNA fragments specific for the Rs-CMV RNA3 sequence.

RT-PCR/DNA sequence determination was performed to analyze the stability of the mutant virus. It was carried out with the Qiagen OneStep RT-PCR kit according to the manufacturer's instructions, using primers flanking of 2b coding region (forward 5′-GTT TGC CTG GTG TTA CGA CAC CGA-3′, reverse 5′-GCG GAT CCT GGT CTC CTT TTG GAG GCC C-3′). PCR products were purified by High Pure PCR product Purification Kit (Roche) prior nucleotide sequence determination.

3. Results and discussion

3.1. Description of the 2b C-terminal structure

So far there is no any published information about the structure of the cucumoviral 2b protein C-terminal domain. However,

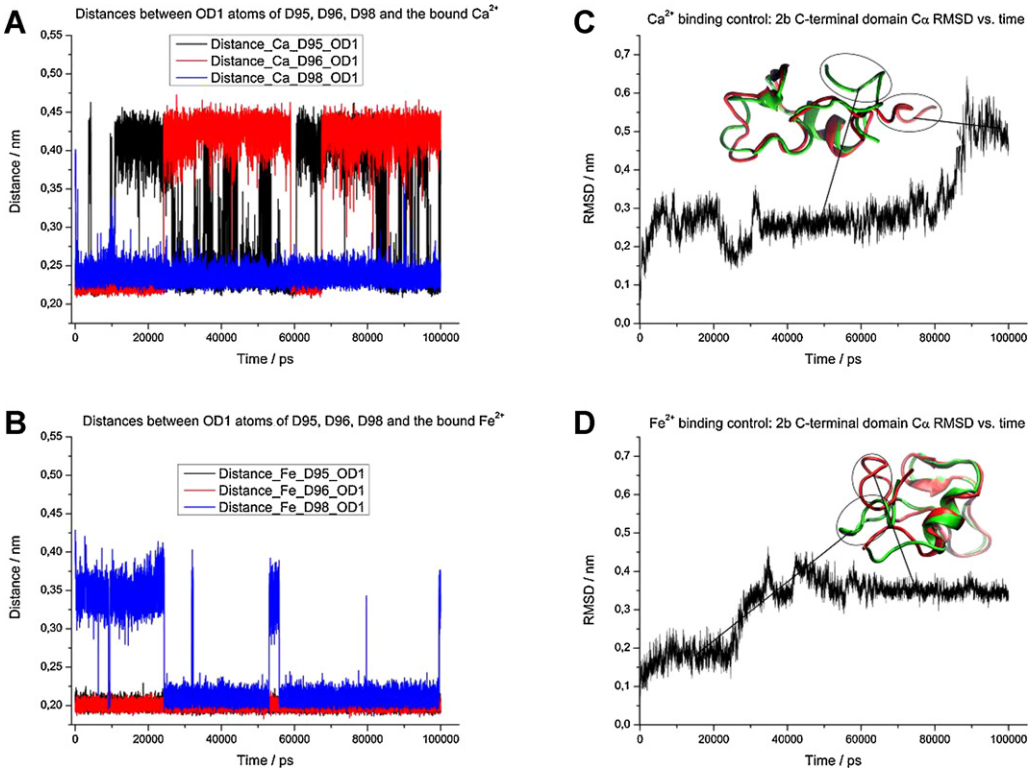

Fig. 6. Analyses of the Ca^{2+} and the Fe^{2+} binding control simulations. Distances between the bound divalent metal ions and the OD1 atoms of the coordinating aspartate side chains (D95, D95, D98) were plotted as a function of time (A and B). The inset ribbon images represent two–two stable conformational states in the course of the control simulations (C and D). The initial structures were taken as references when calculating the RMSD values.

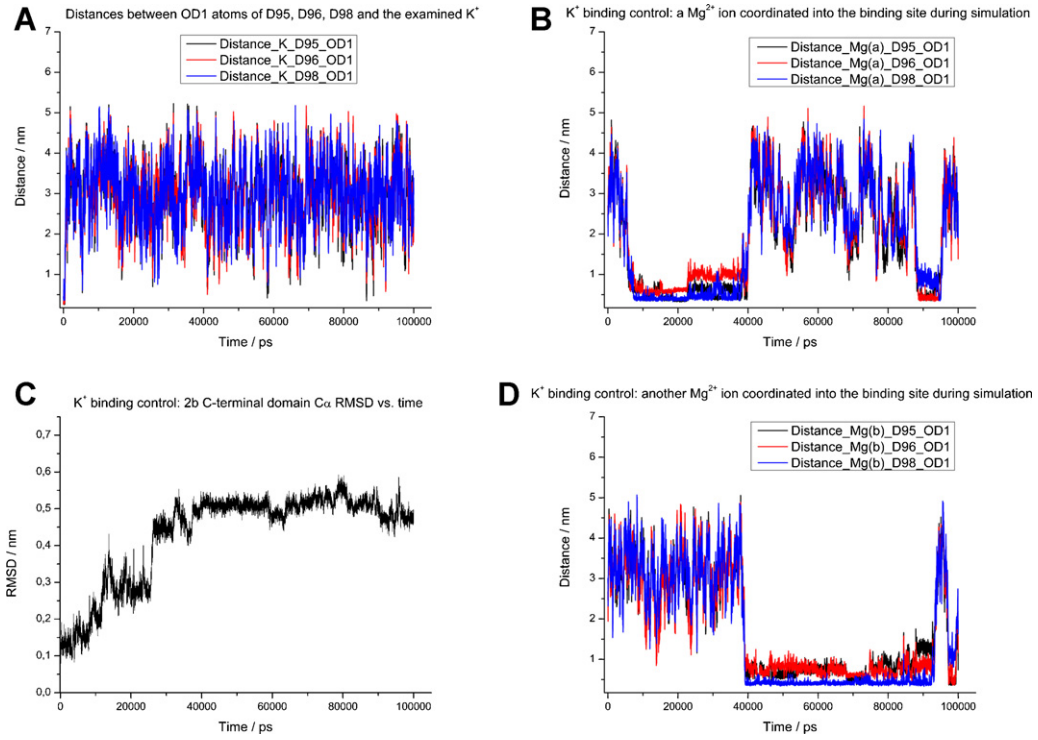

Fig. 7. Analysis of the K^+ binding control. Distances between the initially bound K^+ ion and the OD1 atoms of the D95, D95, D98 were plotted as a function of time (A). The RMSD plot show that the simulated system started to converge into a dynamic equilibrium state after the 30th ns (B). The structural stabilization are due to two Mg^{2+} ions which migrated into the divalent metal ion binding site from the solvent. These ions alternatively occupied the binding site during the control simulation (C and D).

experimental data shows that the partial or total deletion of the C-terminal domain alters the symptom severity and slows down the virus spread within plants [26,27]. The use of the traditional structure–function assignment methods are significantly limited by the fact that the secondary structure prediction methods predict disorder or intrinsically unstructured protein (IUP) region for the CMV 2b protein C-terminal domain. We checked the Rs-CMV 2b protein sequence with PSIPRED and IUPRED servers (http://bioinf.cs.ucl.ac.uk/psipred/, http://iupred.enzim.hu/). However the I-TASSER structure prediction applications predicted a stable, short α-helix between the Ser68 and the Glu76 at the beginning of the C-terminal domain (Fig. 3). This helix remained stable and intact throughout all simulations. The next sequence part produced a typical IUP-like behavior: disordered structures were formed during the simulations without divalent metal ion coordination. In that case where a divalent metal ion is coordinated by Asp95, Asp96 and Asp98 a short β-sheet formed after the C-terminal helix (aa 79–85) which is followed by a loop region (86–94) till the metal ion binding site. Interestingly, in some CMV strains (*e.g.* Trk7 and LY) this loop region is absent from the 2b protein (Fig. 1C). The NCBI/GenBank accession numbers for Trk7 and LY strains are AJ007934 and AF198102, respectively. After the divalent metal ion binding site the C-terminal tail terminates the protein sequence which contains two conservative tryptophan residues. This region formed an elongated α-helix-like structure during MD simulations.

3.2. Metal ion binding screens by MD simulations

Since we found that the C-terminal domain had disorder behavior during MD simulation of the whole siRNA–2b ribonucleoprotein complex and the expected π–π stacking interactions did not evolve between tryptophan residues and terminal siRNA bases, we decided that comprehensive metal ion binding simulation screens will be run in order to identify which type of metal ions can bind permanently to the recently recognized DDTD sequence motif at the 2b C-terminal domain. This motif is located between the 95 and 98 residues and strictly conserved among all CMV isolates. Four divalent metal ions were tested: Ca^{2+}, Mg^{2+}, Fe^{2+} and Zn^{2+}.

The RMSD (root mean square deviation) graphs show that the system which contained Mg^{2+} ion rapidly stabilized the structure of the 2b C-terminal domain in about 15 ns. The RMSD plot starts to converge to a constant function when the system reaches a dynamic equilibrium state. The Mg^{2+} screen reached the dynamic equilibrium state (black line), while we did not observe this effect for the other metal ions and in the case of the Rs2DDTD/95–98/AAAA

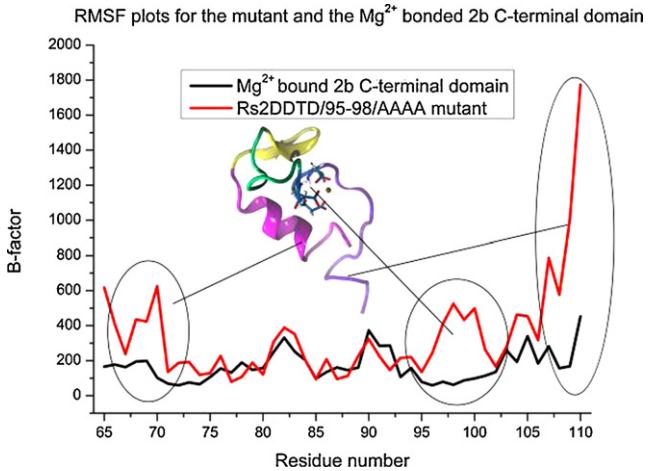

Fig. 8. Thermal factor analysis. RMSF plots of the Rs2DDTD/95–98/AAAA mutant (red line) and Mg^{2+} binding screen (black line) simulations are superimposed. The significant differences are circled and assigned to the appropriate structural elements of the 2b C-terminal domain. (For interpretation of the references to color in this figure legend, the reader is referred to the web version of the article.)

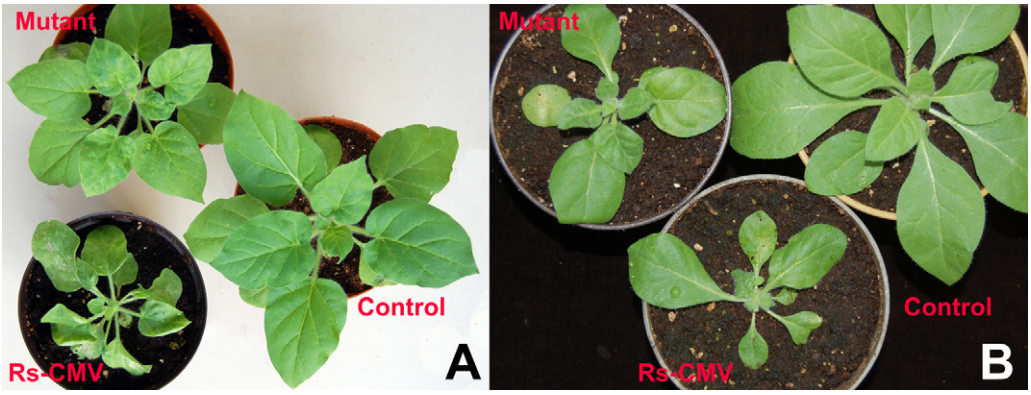

Fig. 9. Typical symptoms elicited 14 days after the inoculation on *N. glutinosa* (A) and on *N. clevelandii* (B) plants by the Rs-CMV and mutated Rs2DDTD/95–98/AAAA virus.

mutant (Fig. 2A). Side chains of Asp95, Asp96 and Asp98 formed a quasi-permanent Mg^{2+} binding site during simulation (Fig. 2B). The other negatively charged residues of the C-terminal domain coordinated metal ions for only short time periods. Fig. 2B and C shows how long was the retention time of the Mg^{2+} ion in the binding site and when it migrates from there, after passing a very short transient state another Mg^{2+} ion binds. (A short video was made from the Mg^{2+} binding which can be seen online.) This is explained by the negative charges of the previously coordinated Asp95, Asp96 and Asp98 side chains accumulated in a small volume generating a large negative electric field, which quickly attracts another Mg^{2+} ion (Fig. 4). The carboxyl oxygen atoms of Asp95, Asp96 and Asp98 were located in the second coordination sphere of the bound Mg^{2+} ion. The first coordination shell was a regular octahedron of water molecules in this simulation, but the carboxyl oxygen atoms may be directly coordinated to the Mg^{2+} ion (Fig. 5A).

3.3. Control simulations

The bound Mg^{2+} was replaced by Ca^{2+}, Fe^{2+} and K^{+} ions to verify the ion selectivity of the putative ion binding site then 100 ns long MD simulations were run for each altered system. In all three cases the ionic strength of the solvent were set with 0.15 M $MgCl_2$. The replaced Ca^{2+} and Fe^{2+} ions remained in the binding site throughout the control simulations. Fig. 6A and B shows that what were the distance between the hydroxylic oxygen atoms (the PDB name is OD1 for this atom type) of the coordinating aspartate carboxyl groups and the bound metal ions. The variation of the distance values (approximately 1.6–2.0 Å) represents the rotation of the carboxyl groups. The larger shifts in the RMSD plots were due to the movement of the C-terminal tail (Fig. 6C and D). In the case of the Ca^{2+} control simulation this C-terminal tail drifting occurred around the 80th ns while in the case of the Fe^{2+} control simulation this conformational jump happened after the 20th ns. In that case when K^{+} ion

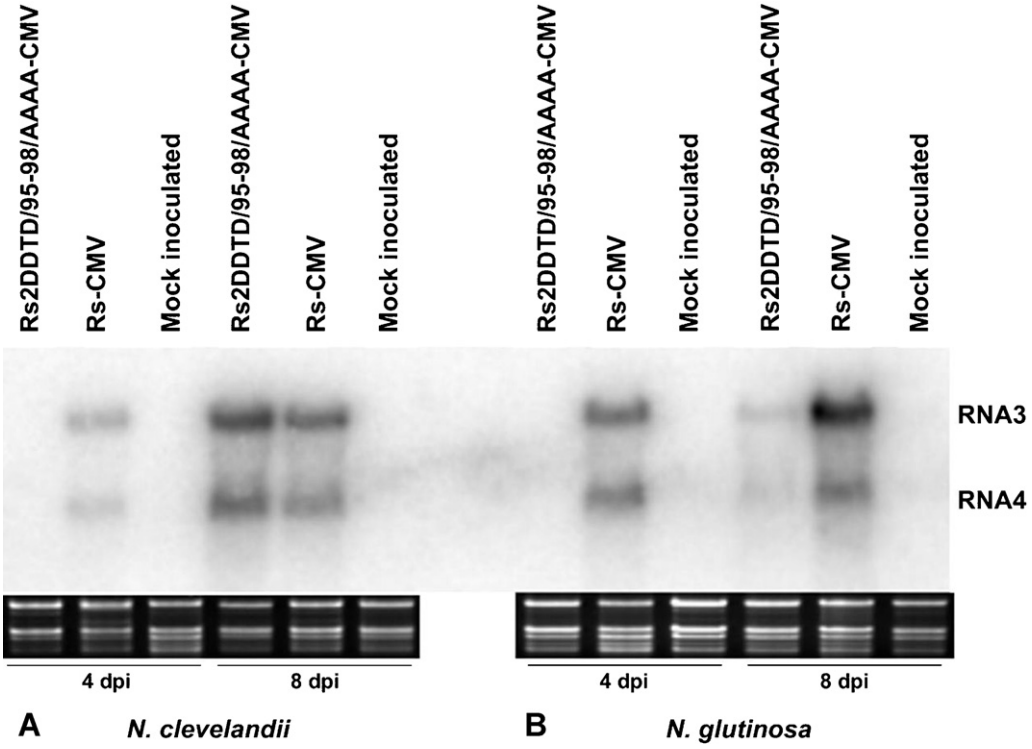

Fig. 10. Northern blot hybridization analysis of total RNAs extracted from non-inoculated leaves. The radiolabeled probe was specific for Rs-CMV RNA3. Ethidium bromide-stained rRNA from the same volume of each sample is shown below each lane. Analysis of *Nicotiana clevelandii* plants 4 and 8 days after inoculation (A). Analysis of *Nicotiana glutinosa* plants 4 and 8 days after inoculation (B).

was placed into the putative metal ion binding site the K^+ immediately moved away from the binding site at the beginning of the simulation (Fig. 7A). The place of the inserted K^+ ion was occupied by Mg^{2+} ion which migrated from the solvent. During the 100 ns long MD simulation two Mg^{2+} occupied alternatively the metal ion binding site (Fig. 7C and D). The structure of the C-terminal domain was stabilized from the 40th ns (Fig. 7B). The calculated RMSF (root mean square fluctuations) values for all residues graphically reflect the stabilizing effect of the divalent metal ion binding on the structure (Fig. 8). There are three significant differences in the RMSF plots between the Rs2DDTD/95–98/AAAA mutant and metal ion bonded simulations. In the course of the mutant simulation the beginning of the short α-helix, the mutated divalent metal ion binding site and the C-terminal tail were more flexible than in the case of the ion bonded simulations. In fact, the short α-helix and the C-terminal tail are close to the aspartate side chains of the metal ion binding site which formed salt-bridges and hydrogen bonds.

3.4. Experimental confirmation

The characterization of the biological impact on symptom development of the 95–98 aa of the 2b protein a mutant virus containing alanine at position 95–98 of the 2b protein was constructed. The symptom characterization of this mutant was carried out on *N. clevelandii* and *N. glutinosa* test plants. Inoculation experiments on both host revealed that systemic symptoms delayed in the case of the Rs2DDTD/95–98/AAAA (quadruple) mutant. While the Rs-CMV induced systemic symptoms 4–6 days post inoculation, the first symptoms appeared only 6–8 days after infection with the quadruple mutant virus. On both test plants inoculated with the quadruple mutant virus the symptoms were milder compared to the symptoms induced by the parental strain. On *N. glutinosa* plants the Rs-CMV causes mosaic, and severe stunting, while the quadruple mutant virus induces mosaic and little or no stunting (Fig. 9A). On *N. clevelandii* plants both the Rs-CMV and the quadruple mutant virus cause mosaic and stunting, but the Rs-CMV induce much stronger stunting and leaf blistering too (Fig. 9B).

The Northern analysis confirmed the visual observation; the systemic movement of the quadruple mutant is delayed. In the non inoculated upper leaves the mutant virus was detected only 8 days after the inoculation. At this time on *N. clevelandii* plants the virus concentration was comparable to the parental strain (Fig. 10A), but on *N. glutinosa* plants the concentration of the quadruple mutant was reduced (Fig. 10B). The RT/PCR sequence determination confirmed the stability of the introduced mutations even 1 month after the inoculation.

3.5. Physiological considerations

The 2b protein carries out its function in the nucleus of plant cells where the two most important divalent cations are the Mg^{2+} and the Ca^{2+}. However, the Ca^{2+} concentration is at least four times smaller than the Mg^{2+} concentration [28]. Therefore, it seems likely that the recently identified divalent ion binding site on the 2b C-terminal domain rather coordinates Mg^{2+} ions, which is also known to play a significant role in stabilizing nucleic acids.

Two other examples show that the Mg^{2+} ion has an important role in enzymatic function and protein structure stabilization. Fig. 5B demonstrates the active site of an enolase enzyme [29]. The Mg^{2+} ion is surrounded by aspartate side chains, water molecules and the 2-phosphoglyceric acid substrate. Fig. 5C exemplifies a carboxylase enzyme active site where glutamate side chains, water molecules and an adenosine-5′-diphosphate moiety coordinate the Mg^{2+} ion [30]. This divalent metal ion binding site in the CMV 2b C-terminal domain is localized directly before the C-terminal tail which contains the Trp99 and Trp105 residues. Due to the conformation stabilizing effect of the bound divalent metal ion the movement of C-terminal tail may become more controllable. Thus, the π–π stacking effect between the aromatic indole rings of Trp99, Trp105 and the basis of the siRNA ends can develop easier and faster. Other enzymatic functions or protein–protein interactions cannot be inferred from these calculations, but there is experimental evidence that 2b protein interferes with RNA silencing by directly blocking the slicer activity of Argonaute1 (AGO1) which is a crucial component of the RNA-induced silencing complex (RISC) [11,31,32].

4. Conclusions

We identified a putative divalent metal ion binding site on the C-terminal domain of CMV 2b protein. The slower movement of the mutant virus construction is supposedly related to the fact that the Rs2DDTD/95–98/AAAA quadruple mutation weakens the stability of the tetramer 2b–siRNA ribonucleo-protein complex. Using these results are going to run a simulation of the entire ribonucleoprotein system, in which the C-terminal stabilizing divalent metal ions are present, this model is closer to reality. Since there is experimental evidence that the 2b protein interacts with the RISC complex, new studies based on our results can be designed in order to get a detailed picture of the 2b protein function. Furthermore, it should be noted that in the case of crystallization of the full-length 2b protein divalent metal ion screen must be carried out in order to avoid disorder in the C-terminus, which may result in unsuccessful crystallization trials.

Acknowledgements

Ákos Gellért was the recipient of a János Bolyai fellowship from the Hungarian Academy of Sciences. The licensing of the Schrödinger Suite software package was funded from the NKTH-OTKA grant under agreement No.: 78317. Thanks are due to Prof. Gábor Náray-Szabó and Dóra Karancsiné Menyhárd for their helpful comments and critical reading of the manuscript. This work was funded partially by the project OTKA K75168. The authors are grateful to P. Salamon for the photos, and the skillful technical assistance of E. Sztánáné Kereszturi is appreciated.

Appendix A. Supplementary data

Supplementary data associated with this article can be found, in the online version, at http://dx.doi.org/10.1016/j.jmgm.2012.08.005.

References

[1] M.H.V. Van Regenmortel, C.M. Faquet, D.H.L. Bishop, E. Carstens, M. Estes, S. Lemon, et al., Virus Taxonomy: Seventh Report of the International Committee on Taxonomy of Viruses, Academic Press, San Diego, 2000.
[2] P. Palukaitis, F. García-Arenal, Cucumoviruses, Advances in Virus Research 62 (2003) 241–323.
[3] U. Melcher, The "30K" superfamily of viral movement proteins, Journal of General Virology 81 (2000) 257–266.
[4] Q. Li, P. Palukaitis, Comparison of the nucleic acid- and NTP-binding properties of the movement protein of Cucumber mosaic cucumovirus and Tobacco mosaic tobamovirus, Virology 216 (1996) 71–79.
[5] M. Suzuki, S. Kuwata, J. Kataoka, C. Masuta, N. Nitta, Y. Takanami, Functional analysis of deletion mutants of cucumber mosaic virus RNA3 using an in vitro transcription system, Virology 183 (1991) 106–113.
[6] R.W. Lucas, S.B. Larson, M.A. Canady, A. McPherson, The structure of tomato aspermy virus by X-ray crystallography, Journal of Structural Biology 139 (2002) 90–102.
[7] T.J. Smith, E. Chase, T. Schmidt, K.L. Perry, The structure of cucumber mosaic virus and comparison to cowpea chlorotic mottle virus, Journal of Virology 74 (2000) 7578–7586.
[8] A.P. Lucy, H.S. Guo, W.X. Li, S.W. Ding, Suppression of post-transcriptional gene silencing by a plant viral protein localized in the nucleus, EMBO Journal 19 (2000) 1672–1680.

[9] G. Brigneti, O. Voinnet, W.X. Li, L.H. Ji, S.W. Ding, D.C. Baulcombe, Viral pathogenicity determinants are suppressors of transgene silencing in Nicotiana benthamiana, EMBO Journal 17 (1998) 6739–6746.
[10] H.W. Li, A.P. Lucy, H.S. Guo, W.X. Li, L.H. Ji, S.M. Wong, et al., Strong host resistance targeted against a viral suppressor of the plant gene silencing defence mechanism, EMBO Journal 18 (1999) 2683–2691.
[11] J. Burgyán, Z. Havelda, Viral suppressors of RNA silencing, Trends in Plant Science 16 (2011) 265–272.
[12] H.Y. Chen, J. Yang, C.Q. Lin, A.Y. Yuan, Structural basis for RNA-silencing suppression by Tomato aspermy virus protein 2b, EMBO Reports 9 (2008) 754–760.
[13] K. Sueda, H. Shimura, A. Meguro, U. Uchida, J. Inaba, C. Masuta, The C-terminal residues of the 2b protein of Cucumber mosaic virus are important for efficient expression in *Escherichia coli* and DNA-binding, FEBS Letters 584 (2010) 945–950.
[14] J.M. Vargason, G. Szittya, J. Burgyánn, T.M. Tanaka Hall, Size selective recognition of siRNA by an RNA silencing suppressor, Cell 115 (2003) 799–811.
[15] J. Burgyán, F. Grieco, M. Russo, A defective interfering RNA molecule in cymbidium ringspot virus-infections, Journal of General Virology 70 (1989) 235–239.
[16] Y. Zhang, I-TASSER server for protein 3D structure prediction, BMC Bioinformatics 9 (2008) 40.
[17] A. Roy, A. Kucukural, Y. Zhang, I-TASSER: a unified platform for automated protein structure and function prediction, Nature Protocols 5 (2010) 725–738.
[18] Schrödinger, LLC, Schrödinger Suite, 101 SW Main Street, Suite 1300 Portland, OR 97204, 2011.
[19] D.E. Shaw, Research, DESMOND, 120 W, 45th St., 39th Fl, New York, NY 10036, 2011.
[20] N.A. Baker, D. Sept, S. Joseph, M.J. Holst, J.A. McCammon, Electrostatics of nanosystems: application to microtubules and the ribosome, Proceedings of the National Academy of Sciences 98 (2001) 10037–10041.
[21] M.K. Gilson, K.A. Sharp, B. Honig, Calculating electrostatic interactions in biomolecules: method and error assessment, Journal of Computational Chemistry 9 (1987) 327–335.
[22] W. Humphrey, A. Dalke, K. Schulten, VMD – visual molecular dynamics, Journal of Molecular Graphics 14 (1996) 33–38.
[23] Z. Divéki, K. Salánki, E. Balázs, The necrotic pathotype of the cucumber mosaic virus (CMV) Ns strain is solely determined by amino acid 461 of the 1a protein, Molecular Plant–Microbe Interactions 17 (2004) 837–845.
[24] J.L. White, J.M. Kaper, A simple method for detection of viral satellite RNAs in small tissue samples, Journal of Virological Methods 23 (1989) 83–94.
[25] J. Sambrook, E.F. Fritsch, T. Maniatis, Molecular Cloning: A Laboratory Manual, 2nd ed., Cold Spring Harbor Laboratory Press, Cold Spring Harbour, 1989.
[26] M. Lewsey, M. Surette, F.C. Robertson, H. Ziebell, S.H. Choi, K.H. Ryu, et al., The role of the Cucumber mosaic virus 2b protein in viral movement and symptom induction, Molecular Plant–Microbe Interactions: MPMI 22 (2009) 642–654.
[27] M.G. Lewsey, I. Gonzalez, N.O. Kalinina, P. Palukaitis, T. Canto, J.P. Carr, Symptom induction and RNA silencing suppression by the cucumber mosaic virus 2b protein, Plant Signaling and Behavior 5 (2010) 705–708.
[28] I.L. Cameron, K.E. Hunter, N.K. Smith, The subcellular concentration of ions and elements in thin cryosections of onion root meristem cells. An electron-probe EDS study, Journal of Cell Science 72 (1984) 295–306.
[29] E.C. Schulz, M. Tietzel, A. Tovy, S. Ankri, R. Ficner, Structure analysis of Entamoeba histolytica enolase, Acta Crystallographia Section D 67 (2011) 619–627.
[30] C.Y. Chou, L. Tong, Structural and biochemical studies on the regulation of biotin carboxylase by substrate inhibition and dimerization, Journal of Biological Chemistry 286 (2011) 24417–24425.
[31] X. Zhang, Y.R. Yuan, Y. Pei, S.S. Lin, T. Tuschl, D.J. Patel, et al., Cucumber mosaic virus-encoded 2b suppressor inhibits Arabidopsis Argonaute1 cleavage activity to counter plant defense, Genes and Development 20 (2006) 3255–3268.
[32] L. Lakatos, G. Szittya, D. Silhavy, J. Burgyan, Molecular mechanism of RNA silencing suppression mediated by p19 protein of tombusviruses, EMBO Journal 23 (2004) 876–884.